

# Unambiguous identification of N-containing oxygenated organic molecules using CI-Orbitrap in an eastern Chinese megacity

Yiqun Lu<sup>1,2</sup>, Yingge Ma<sup>1</sup>, Dan Dan Huang<sup>1</sup>, Shengrong Lou<sup>1</sup>, Sheng'ao Jing<sup>1</sup>, Yaqin Gao<sup>1</sup>, Hongli Wang<sup>1</sup>, Yanjun Zhang<sup>3</sup>, Hui Chen<sup>4</sup>, Yunhua Chang<sup>5</sup>, Naiqiang Yan<sup>2</sup>, Jianmin Chen<sup>4</sup>, Christian George<sup>3</sup>, Matthieu Riva<sup>3</sup>, Cheng Huang<sup>1\*</sup>

<sup>1</sup> State Environmental Protection Key Laboratory of Formation and Prevention of Urban Air Pollution Complex, Shanghai Academy of Environmental Sciences, Shanghai 200233, China;

<sup>2</sup> School of Environmental Science and Engineering, Shanghai Jiao Tong University, Shanghai 200240, China

<sup>3</sup> Univ. Lyon, Université Claude Bernard Lyon1, CNRS, IRCELYON, 69626 Villeurbanne, France;

<sup>4</sup> Shanghai Key Laboratory of Atmospheric Particle Pollution and Prevention (LAP<sup>3</sup>), Department of Environmental Science & Engineering, Jiangwan Campus, Fudan University, Shanghai 200438, China

<sup>5</sup> Collaborative Innovation Center on Forecast and Evaluation of Meteorological Disasters (CIC-FEMD), NUIST Center on Atmospheric Environment, Nanjing University of Information Science and Technology, Nanjing 210044, China

## Contents of this file

Section S1 to S3

Figures S1 to S9

Table S1 to S2

**Figure S1.** The map of the field site (Shanghai Academy of Environmental Sciences) that is a representative urban station.

**Figure S2.** Timeseries of key measurements during the field campaign.

**Figure S3.** Mathematical diagnostics of PMF solutions, including the overall changes of  $Q/Q_{\text{exp}}$  and the explained variation from two-factor to nine-factor solutions. For each number of factors, five seed runs were performed to test the consistency of the solution.

**Figure S4.** Timeseries of factors in 2-6 factor solutions of PMF. The panels from top to bottom are 2-factor solution, 3-factor solution, 4-factor solution, 5-factor solution and 6-factor solution, respectively.

27 **Figure S5.** Diel variation patterns of factors in 2-6 factor solutions of PMF. The panels from top to bottom are 2-factor solution, 3-factor solution, 4-  
28 factor solution, 5-factor solution and 6-factor solution, respectively.

29 **Figure S6.** The factor profiles in the six-factor solution.

30 **Figure S7.** The relative contributions of OOMs with different carbons to the extremely low-volatility organic compounds (ELVOC,  $C^* < 3 \times 10^{-5} \mu\text{g}$   
31  $\text{m}^{-3}$ ) and low-volatility organic compounds (LVOC,  $3 \times 10^{-5} \leq C^* < 3 \times 10^{-1} \mu\text{g m}^{-3}$ ).

32 **Figure S8.** Timeseries of  $\text{N}_2\text{O}_5$  concentration (top panel), estimated  $\text{NO}_3$  concentration (middle panel), and the nighttime factor-1 (bottom panel).

33 **Figure S9.** Timeseries of  $\text{PM}_{2.5}$  concentration (top panel), and the episode factor-1 (bottom panel).

## 34 **S1. Other ancillary measurements**

35 The mass concentration of ambient particles was measured by particle monitor (TEOM 1405DF, Thermo,  
36 USA). SO<sub>2</sub>, O<sub>3</sub> and NO<sub>x</sub> concentrations were measured using a SO<sub>2</sub> analyzer (Model 43i, Thermo, USA), a O<sub>3</sub>  
37 analyzer (Model 49i, Thermo, USA) and a NO<sub>x</sub> analyzer (Model 42i, Thermo, USA) with the detection limits of  
38 0.1 ppbv, 0.5 ppbv and 0.4 ppbv, respectively. The above instruments were pre-calibrated before the campaign. The  
39 solar radiation was measured on the rooftop of the building. Atmospheric N<sub>2</sub>O<sub>5</sub> concentrations were measured by  
40 an iodide CI-API-TOF. The concentrations of NO<sub>3</sub> radicals were estimated under the assumption that NO<sub>3</sub>, NO<sub>2</sub> and  
41 N<sub>2</sub>O<sub>5</sub> could reach an equilibrium quickly in tropospheric conditions (Brown and Stutz, 2012). The total  
42 concentrations of VOC precursors (TVOC) were determined by the measurement of an online GC-MS (7890A-  
43 5975C, Agilent, USA).

## 44 **S2. Overview of the campaign**

45 An overview of the measurement data, illustrating the air quality as well as the meteorological  
46 conditions (global radiation, temperature, wind direction, wind speed, and RH), concentrations of trace  
47 gases and pollutants (PM<sub>2.5</sub>, O<sub>3</sub>, NO<sub>x</sub>, N<sub>2</sub>O<sub>5</sub>, and TVOCs) during the campaign, is provided in this section  
48 as shown in Figure S2 and Table S1. Firstly, the maximum intensities of global radiation on individual  
49 days were in a range of 637-867 W m<sup>-2</sup>, indicating strong photochemical activities during the daytime of  
50 the campaign. The relative humidity (RH) exhibited a clear diurnal variation pattern with a range of 21-  
51 91% . The wind (0-7 m/s) from the north to northeast prevailed during the campaign and frequently  
52 resulted in increased PM<sub>2.5</sub> concentrations due to the transport. The PM<sub>2.5</sub> concentration were in a range  
53 of 6-59 µg m<sup>-3</sup> (5-95 % percentile). The 5-95 % percentile ranges of [O<sub>3</sub>], [NO<sub>x</sub>], and [TVOC] were 4.6-  
54 58.6 ppbv, 8.9-69.6 ppbv, and 15.2-77.5 ppbv, respectively. O<sub>3</sub> showed an obvious diurnal variation,  
55 peaking at 13:00 – 15:00. Diurnal variations of NO<sub>x</sub> and TVOC showed high concentrations over the rush  
56 hours. A PM episode with mean PM<sub>2.5</sub> concentration of 56.4 µg m<sup>-3</sup> occurred from November 6<sup>th</sup> to  
57 November 8<sup>th</sup>, accompanied by a high concentration of both TVOC and NO<sub>x</sub>, indicating the same origins  
58 of air pollutants. While the N<sub>2</sub>O<sub>5</sub> remained in low concentration levels in general, three peak

59 concentrations up to about 600 pptv appeared at nighttime during November 6<sup>th</sup>-8<sup>th</sup>.

### 60 **S3. Positive matrix factorization (PMF)**

61 Positive matrix factorization (PMF) allows for time-resolved mass spectra to be expressed as a linear  
62 combination of a finite number of factors, assuming that the factor profiles are constant and unique. Since  
63 this method does not require a priori information about the factors, it is an ideal technique for extracting  
64 information from ambient measurements where the detailed chemistry, sources, and atmospheric  
65 processes are complex. PMF has already been used in source apportionment analysis of OOMs in previous  
66 studies (Yan et al., 2016; Zhang et al., 2019, 2022). In this study, PMF was performed using the Igor-based  
67 interface Source Finder (SoFi, v6.3), run by the multilinear engine (ME-2) (Canonaco et al., 2013). The  
68 data for the PMF model inputs were prepared according to the method described in previous studies  
69 (Zhang et al., 2022). Note that the orbitrap analyzer does not measure signal below a certain threshold  
70 resulting in incomplete time series for species present at low concentration level. Therefore, the species  
71 characterized by incomplete time series with more than 90% missing data and the spectra with more than  
72 80% missing were removed (Zhang et al., 2022).

73 PMF analysis in this work was performed in 2-10 factors as shown in Figure S3. Five runs for each  
74 solution show good consistencies in both  $Q/Q_{exp}$  and explained variation, indicating the small model  
75 uncertainty. The change of  $Q/Q_{exp}$ , which decreases stepwise from 2.61 (assuming two factors) to 0.65  
76 (assuming nine factors). Since the absolute value of  $Q/Q_{exp}$  might be misleading, the trend of  $Q/Q_{exp}$  is  
77 useful to determine the minimum factor number (Ulbrich et al., 2009), a large decrease in  $Q/Q_{exp}$  indicates  
78 that the additional factor may explain a large fraction of unaccounted variability in the data. The third  
79 factor significantly decreases the  $Q/Q_{exp}$  value from 2.61 to 1.83, suggesting the importance of the third  
80 factor. By adding the third factor, the model can explain 79.4 % of the data variation, in comparison to  
81 75.4 % when only two factors are assumed. This improvement in model performance also implies the  
82 addition of third factor is crucial. The second largest increase in the explained fraction (from 79.4 % to  
83 81.3 %) happens when adding the fourth factor and the  $Q/Q_{exp}$  value decreases from 1.83 to 1.51. When  
84 model contains 5, 6, 7, 8, 9 and 10 factors, the  $Q/Q_{exp}$  values are about 1.27, 1.07, 0.94 and 0.83, 0.73

85 and 0.66 respectively while the explained fraction by mode are in a range of 82.9-87.5 %.

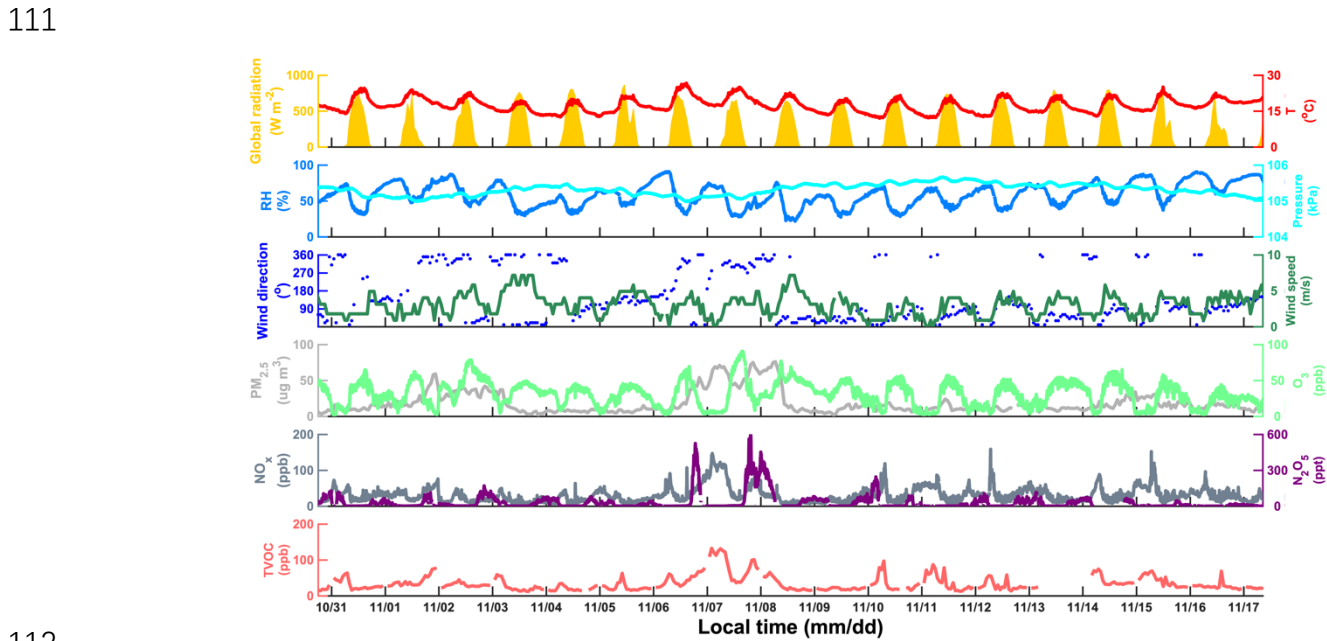
86 Since the PMF analysis is a pure mathematical method without any prior physical or chemical  
87 assumptions, choosing the best factor number is critical before describing the PMF results. In terms of  
88 trends, more factors would get more freedom to follow subtle variations of the matrix, however, artificially  
89 choosing too many factors will over analyze the matrix, resulting in the split of physically meaningful  
90 source apportionment into meaningless ones. The timeseries and diurnal variations of factors are shown  
91 in Figure S4 and Figure S5. The two-factor solution leads to a distinct daytime factor and a night factor.  
92 In the three-factor solution, the timeseries of first two factors are more or less the same as those in the  
93 two-factor case, but the variation pattern of second factor has changed in the daytime, the new factor tracks  
94 the PM<sub>2.5</sub> concentration well in two PM episodes, and exhibits a ush-hour peak in the morning. The four-  
95 factor solution results in two daytime factors originated from the old daytime factor. When five factors are  
96 assumed, an additional nighttime factor appears. When six factors are assumed, an afternoon rush-hour  
97 factor appears. For seven factors, the derived new factor has no strong correlation with any independent  
98 tracer. Herein, we concluded that the PMF solution with six factors is the optimal solutions and chose  
99 to limit our further analysis to the six-factor solution because it is not possible to distinguish the  
100 identification of “real” factors without significant correlations. The factor profiles in the six-factor solution  
101 could be seen in Figure S6.

102 In the aspect of variation patterns, we classify the six factors into three types. The first two factors  
103 are related to the daytime photochemical activities and defined as daytime factor-1 and daytime factor-2.  
104 The third factor and fourth factor show clear nocturnal patterns and defined as nighttime factor-1 and  
105 nighttime factor-2. The fifth factor and the sixth factor are more related to the emission episode and thus  
106 defined as episode factor-1 and episode factor-2. Table S1 shows the peak times and fingerprint molecules  
107 of the factors.

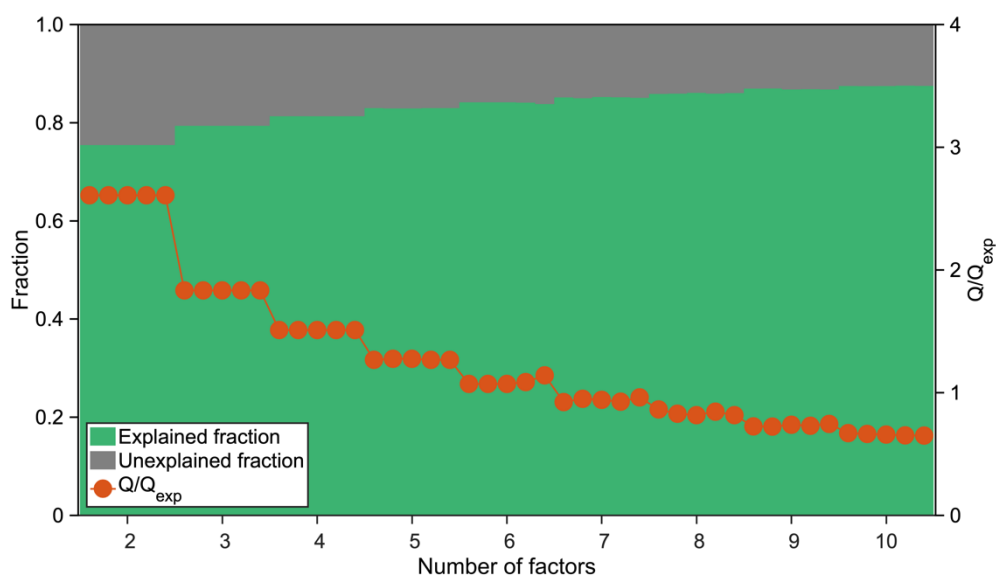
108



109  
 110 **Figure S1.** The map of the field site (Shanghai Academy of Environmental Sciences) that is a representative urban station.

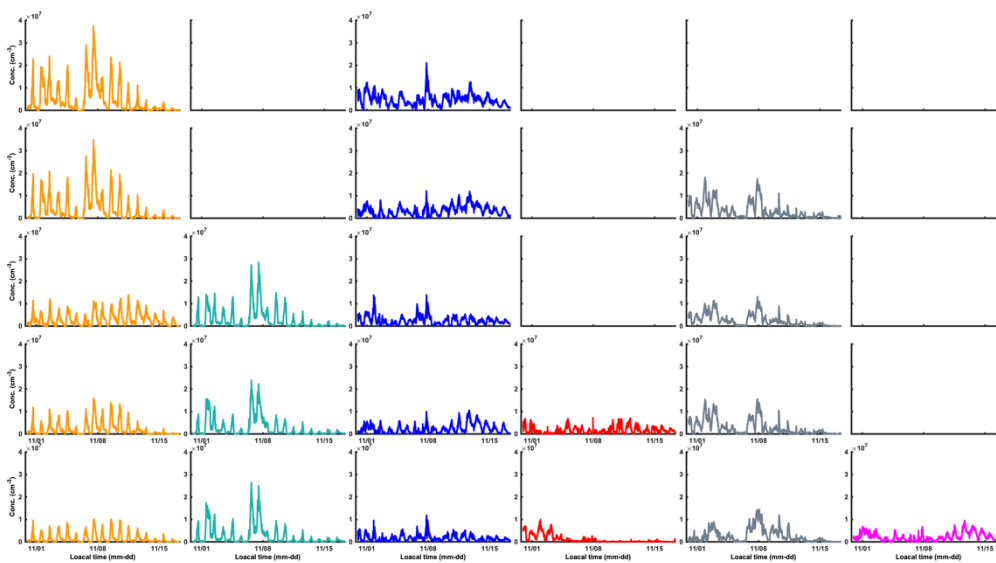


112  
 113 **Figure S2.** Timeseries of key measurements during the field campaign.



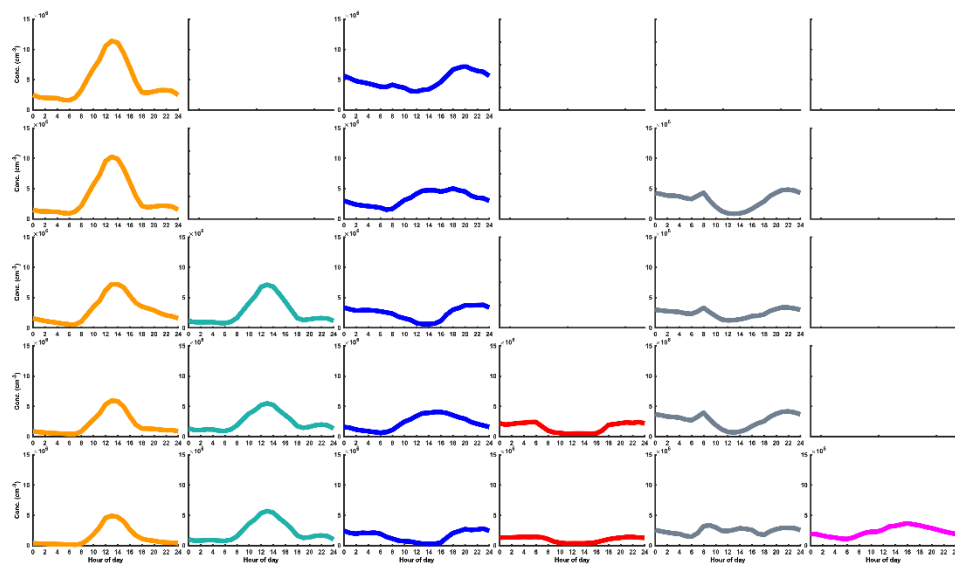
115  
116  
117  
118  
119

**Figure S3.** Mathematical diagnostics of PMF solutions, including the overall changes of  $Q/Q_{exp}$  and the explained variation from two-factor to nine-factor solutions. For each number of factors, five seed runs were performed to test the consistency of the solution.



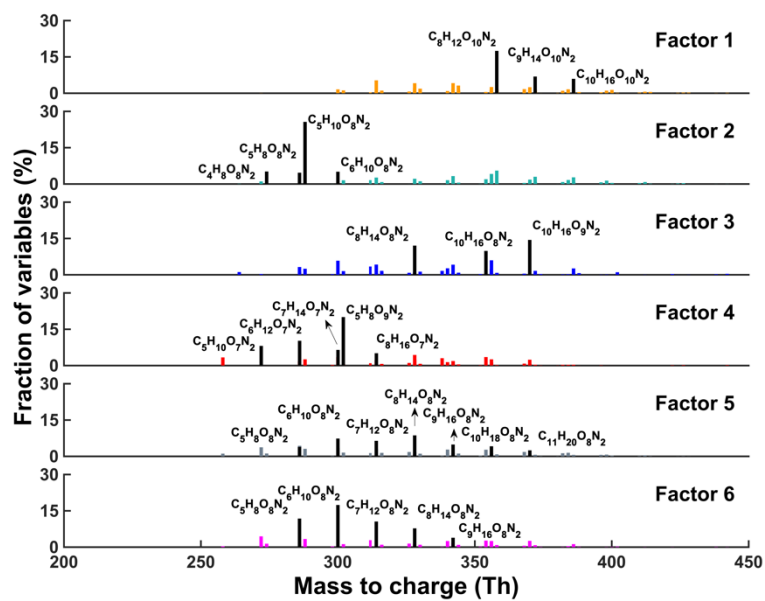
120  
121  
122

**Figure S4.** Timeseries of factors in 2-6 factor solutions of PMF. The panels from top to bottom are 2-factor solution, 3-factor solution, 4-factor solution, 5-factor solution and 6-factor solution, respectively.



123  
124  
125

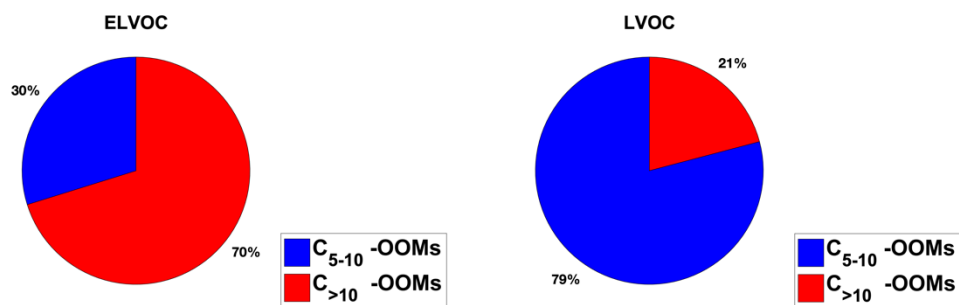
**Figure S5.** Diel variation patterns of factors in 2-6 factor solutions of PMF. The panels from top to bottom are 2-factor solution, 3-factor solution, 4-factor solution, 5-factor solution and 6-factor solution, respectively.



126  
127

**Figure S6.** The factor profiles in the six-factor solution, the black ones represent fingerprint molecules.





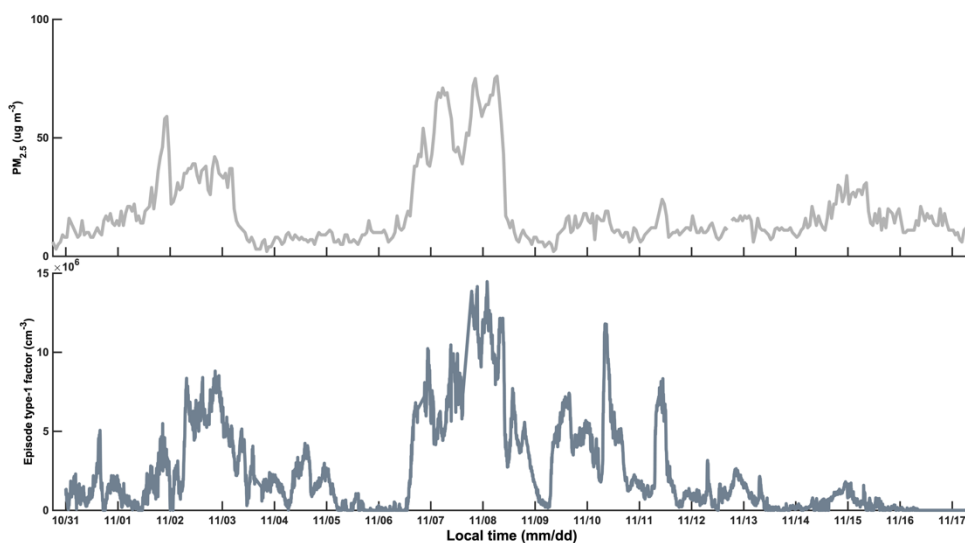
128

129

130

131

**Figure S7.** The relative contributions of OOMs with different carbons to the extremely low-volatility organic compounds (ELVOC,  $C^* < 3 \times 10^{-5} \mu\text{g m}^{-3}$ ) and low-volatility organic compounds (LVOC,  $3 \times 10^{-5} \leq C^* < 3 \times 10^{-1} \mu\text{g m}^{-3}$ ).

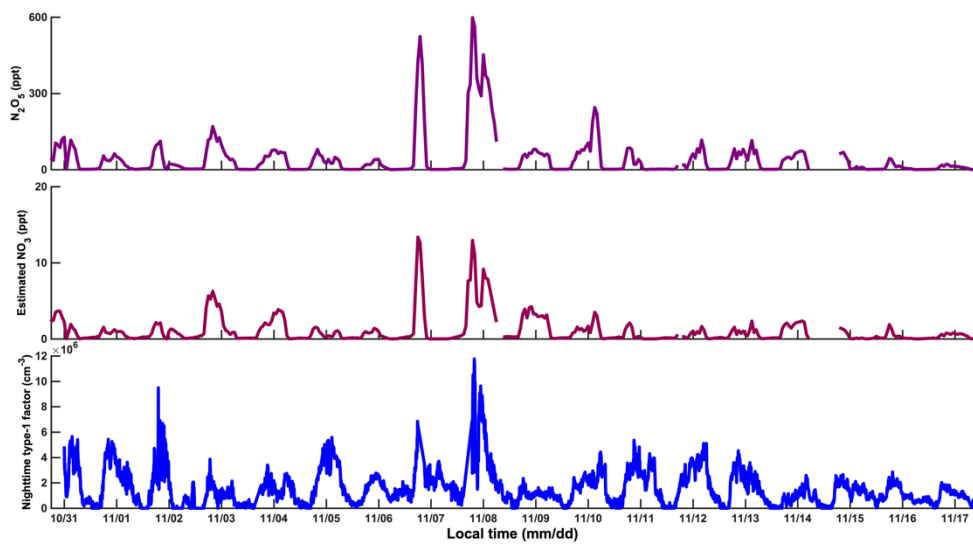


132

133

**Figure S8.** Timeseries of PM<sub>2.5</sub> concentration (top panel), and the episode factor-1 (bottom panel).

134



135

136

137

**Figure S9.** Timeseries of  $N_2O_5$  concentration (top panel), estimated  $NO_3$  concentration (middle panel), and the nighttime factor-1 (bottom panel).

Table S1 Summary of the Factors in six-factor solution

Factor	Factor	Peak time	Fingerprint molecules
Daytime	Daytime factor-1	12:00-14:00	$C_nH_{2n-4}O_{10}N_2$ (n=8-10)
	Daytime factor-2	12:00-14:00	$C_nH_{2n}O_8N_2$ (n=4-5), $C_nH_{2n-2}O_8N_2$ (n=5-6)
Nighttime	Nighttime factor-1	19:00-23:00	$C_{10}H_{16}O_9N_2$ , $C_{10}H_{16}O_8N_2$ , $C_8H_{14}O_8N_2$
	Nighttime factor-2	20:00-06:00	$C_5H_8O_9N_2$ , $C_nH_{2n}O_7N_2$ (n=5-8)
Episode	Episode factor-1	PM episode	$C_nH_{2n-2}O_8N_2$ (n=5-11)
	Episode factor-2	Afternoon rush-hour (16:00)	$C_nH_{2n-2}O_8N_2$ (n=5-9)

Table S2 Averaged  $nO_{\text{eff}}$  of 2N-OOMs in the four cases

Case	$\overline{[2N - OOM_{Aro}]}$	$\overline{[2N - OOM_{Ali}]}$	$\overline{[2N - OOM_{MT}]}$	$\overline{[2N - OOM_{Total}]}$
CL <sub>day</sub>	5.6	4.0	4.8	4.6
CL <sub>night</sub>	4.8	3.9	4.6	4.2
PL <sub>day</sub>	5.3	4.0	4.9	4.3
PL <sub>night</sub>	4.8	3.9	4.5	4.1

## Reference

- Brown, S. S. and Stutz, J.: Nighttime radical observations and chemistry, *Chem. Soc. Rev.*, 41, 6405–6447, doi:10.1039/c2cs35181a, 2012.
- Canonaco, F., Crippa, M., Slowik, J. G., Baltensperger, U. and Prévôt, A. S. H. H.: SoFi, an IGOR-based interface for the efficient use of the generalized multilinear engine (ME-2) for the source apportionment: ME-2 application to aerosol mass spectrometer data, *Atmos. Meas. Tech.*, 6(12), 3649–3661, doi:10.5194/amt-6-3649-2013, 2013.
- Ulbrich, I. M., Canagaratna, M. R., Zhang, Q., Worsnop, D. R. and Jimenez, J. L.: Interpretation of organic components from Positive Matrix Factorization of aerosol mass spectrometric data, *Atmos. Chem. Phys.*, 9(9), 2891–2918, doi:10.5194/acp-9-2891-2009, 2009.
- Yan, C., Nie, W., Äijälä, M., Rissanen, M. P., Canagaratna, M. R., Massoli, P., Junninen, H., Jokinen, T., Sarnela, N., Häme, S. A. K., Schobesberger, S., Canonaco, F., Yao, L., Prévôt, A. S. H., Petäjä, T., Kulmala, M., Sipilä, M., Worsnop, D. R. and Ehn, M.: Source characterization of highly oxidized multifunctional compounds in a boreal forest environment using positive matrix factorization, *Atmos. Chem. Phys.*, 16, 12715–12731, doi:10.5194/acp-16-12715-2016, 2016.
- Zhang, Y., Peräkylä, O., Yan, C., Heikkinen, L., Äijälä, M., Daellenbach, K. R., Zha, Q., Riva, M., Garmash, O., Junninen, H., Paatero, P., Worsnop, D. and Ehn, M.: A novel approach for simple statistical analysis of high-resolution mass spectra, *Atmos. Meas. Tech.*, 12(7), 3761–3776, doi:10.5194/amt-12-3761-2019, 2019.
- Zhang, Y., Li, D., Ma, Y., Dubois, C., Wang, X., Perrier, S., Chen, H., Wang, H., Jing, S., Lu, Y., Lou, S., Yan, C., Nie, W., Chen, J., Huang, C., George, C. and Riva, M.: Field Detection of Highly Oxygenated Organic Molecules in Shanghai by Chemical Ionization–Orbitrap, *Environ. Sci. Technol.*, doi:10.1021/acs.est.1c08346, 2022.